

## FORMATION AND BEHAVIOR OF SURFACE LAYERS ON ELECTRON EMISSION GLASSES

A.M. THEN and C.G. PANTANO

*Department of Materials Science and Engineering, The Pennsylvania State University, University Park, PA 16802, USA*

The thermochemical reduction of thin surface layers on multicomponent lead-silicate glasses is fundamental to their use in electron multiplier and microchannel plate devices. These surface layers can exhibit a specific conductivity as high as  $10^{-2} (\Omega \text{ cm})^{-1}$  and secondary electron yields up to 3.5. However, due to the complex processing used in the fabrication of the devices, a basic understanding of the chemical and structural surface characteristics responsible for these properties has not been established. Moreover, the effects of prolonged electron bombardment upon the chemical characteristics of the surface have not been extensively investigated, nor related to any associated degradation of the electron emission properties.

In this study, the clean fracture surfaces of these glasses were investigated. The effects of hydrogen reduction, chemical etching, and prolonged electron bombardment were determined. Ion-scattering spectroscopy (ISS) was used for its monolayer sensitivity, especially to alkali species, while secondary ion mass spectroscopy (SIMS) provided depth profiles. The hydrogen profile created by the reduction could also be obtained with SIMS. X-ray photoelectron spectroscopy (XPS) was employed selectively to examine changes in the oxidation state of the surface species.

It was found that the hydrogen reduction of these glasses creates a thin 20–50 nm silica-rich surface layer. The layer of reduced lead atoms is beneath this zone, and is visible to depths of the order 5  $\mu\text{m}$ , but the hydrogen profiles which are found in these surfaces extend only 0.5  $\mu\text{m}$  in depth. The electron bombardment of these surfaces leads to a decrease in concentration of alkali and lead in the surface monolayer, and to a change in the hydrogen profile. The cross-section for this bombardment-induced change in the surface composition correlates with the reported gain degradation in microchannel plate devices.

### 1. Introduction

It is well known that when silicate glasses containing large amounts of lead oxide are treated in hydrogen at elevated temperatures, a (semi)conducting surface layer is formed [1–4]. The glass surface layer appears black due to the formation of dispersed Pb particles during the thermochemical reduction of PbO in hydrogen. The thickness and resistivity of this layer depends upon the heat treatment conditions, but are typically in the range 0.1–10  $\mu\text{m}$  and  $10^2$ – $10^{10} \Omega \text{ cm}$ , respectively. There have, of course, been many studies of the composition, structure, and electrical properties of this surface layer [5–26]. The source of the electrical conductivity within these surface layers has been reviewed in some detail by Trap [22]; he claims that there are both ionic and electronic contributions to the conductivity. Many authors have discussed the conduction mechanism in more detail.

Some have suggested that the metallic lead particles are fundamental to a tunnelling [24,25] or percolation [26] mechanism. Others have proposed that an intermediate metastable species ( $\text{Pb}^+$ ) which is produced by the reduction, acts as an electron donor and is responsible for hopping semi-conduction [23]. Nevertheless, the conduction mechanism has not been fully defined nor has its relationship to the processing conditions and surface layer characteristics been established.

The secondary electron yield characteristics of the surface layer on these treated glasses is the basis for their widespread application in electron multiplier and microchannel plate devices [27–30]. The secondary electron yield is influenced, predominantly, by the work function of the surface and the inelastic mean free path of the electrons. It is important to recognize that whereas the conductivity of the surface layer may extend over depths of hundreds to thousands of ångströms, the

secondary electrons are created within tens to hundreds of ångströms from the surface. In fact, it is possible that the secondary electron yield of the surface does not depend in any direct way on the presence of a conductive surface layer [30]. The conductivity may be important only to the extent that it influences the device operation. Hill [7] has attributed the high secondary electron yield of these glasses to the presence of alkali, specifically potassium, which segregates to the surface. This effect of potassium is not surprising considering the use of other electropositive metals such as cesium and osmium in the creation of low work function surfaces. Of course, an important issue in the performance of electron multipliers and micro-channel plates is the stability of the alkali in the glass surface layer – especially under the electron irradiation – which is fundamental to the long-term operation of these devices.

In this study, clean fracture surfaces were treated to determine the effects of hydrogen reduction upon the surface composition of two different alkali–lead silicate glasses – one containing potassium and rubidium and the other containing cesium and rubidium. This approach is in contrast to the work already reported in the literature [5–26] where polished and/or chemically processed surfaces were often examined. Also, many of the reported surface analyses were performed with Auger electron spectroscopy, wherein electron beam effects can severely affect the surface of interest. Here, low-energy ion-scattering spectroscopy (ISS) was used to analyze the surfaces because of its monolayer sensitivity to alkali; clean fracture surfaces created in vacuum provided a reference for interpretation of the treated surfaces. Secondary ion mass spectroscopy (SIMS) provided in-depth profiles of the surface – especially for hydrogen. The compositional stability of these surfaces during prolonged electron beam bombardment was also measured to gain insight about the mechanisms of degradation in the secondary electron yield. The surfaces were irradiated – in situ – within the vacuum chamber where ISS could be used to monitor periodically the alkali and lead surface concentration. The clean smooth fracture surfaces used in these experiments provided information intrinsic to the bulk glass com-

position, the hydrogen reduction process, and the electron irradiation effects. However, in the fabrication of real devices, the surfaces are initially acid etched. Thus, the effects of acid etching were also examined.

## 2. Experimental methods

One of the glasses used in this study was Corning Code 8161 – 52% PbO, 39% SiO<sub>2</sub>, 5% K<sub>2</sub>O, 2% Rb<sub>2</sub>O and 2% BaO. The other glass was a modification of 8161 wherein all of the potassium was replaced by cesium and additional barium and rubidium. The bulk glasses were cut into bars to facilitate the creation of smooth, flat fracture surfaces. Some of the bars were fractured in ultra-high vacuum to provide reference standards for the ISS analyses and the electron-beam irradiation studies. Otherwise, they were fractured in air immediately before the surface treatments. The surface treatments were carried out in a commercial clean-room environment. The acid etch was brief and utilized an ~0.10 N HCl solution. The hydrogen reduction took ~10 h at 450–500 °C. These conditions are virtually identical to those used in the fabrication of secondary electron emission devices.

The ISS analyses (Model 520-Kratos) utilized <sup>4</sup>He<sup>+</sup> at 1500 eV; the beam diameter was ≈ 1 mm and the beam current ≈ 0.20 μA. The scan time per spectra was about 30 s and so only a negligible amount of sputtering occurred during the data acquisition; the effective sputter rate was < 6 nm/h. The build-up of positive surface charge was eliminated through the use of a neutralizing electron filament which was placed near the sample surface. A feedback loop based upon the sample current was used to control the surface potential.

The SIMS analyses (Cameca IMS-3F) were performed using an <sup>18</sup>O<sup>-</sup> beam at 17.5 keV; the negative primary ions minimize the charging problems which often plague SIMS depth profiling of insulators. A 125 μm beam was rastered over a 350 μm × 350 μm area at ≈ 100 nA. A 60 μm diameter aperture was used to eliminate edge effects. The sputter rate was obtained by measuring the crater depths with a profilometer. In these

analyses, a sputtering rate of  $86 \text{ \AA}/\text{min}$  was typical. A quantitative analysis of the hydrogen concentration was achieved using an ion implant standard; the implant standard was prepared using the (Cs,Rb)-glass in the unreduced state.

The XPS analyses (Surface Science Laboratories Small-Spot XPS) used Al  $K\alpha$  X-rays. The spectra were normalized to the Si 2p binding energy (at 103.4 eV) and the integrated intensity of the Si 2p line. The ion sputtering was performed with 1 keV  $\text{Ar}^+$ .

The electron irradiation studies were carried out in the ISS system at a vacuum level of  $\approx 1 \times 10^{-8}$  Torr. The electron beam (Model EG5-VSW Scientific Instruments) was rastered over a  $5 \text{ mm} \times 5 \text{ mm}$  area at a TV scan rate. The beam was 500 eV and the current density was  $1\text{--}5 \times 10^{-6} \text{ A}/\text{cm}^2$ .

The spectra and depth profiles could be reproduced to within 1 or 2% between various regions on each specimen, and in the case of specimens processed together, between surfaces on different specimens. However, there were variations in the data of up to 10 or 20% when specimens prepared in different processing runs were examined. These differences were due to variations in the process control, but nevertheless did not alter the important features of the surface nor the model proposed to describe these surfaces.

### 3. Results

#### 3.1. Surface characteristics

The most obvious effect of the heat treatment in hydrogen is blackening of the surface. Unfortunately, the thickness of the *black* surface layer is not easily obtained, even after the glasses have been cut into thin cross-sections for examination in the optical microscope. Nevertheless, in the TEM one can observe electron dense particles, approximately 10 nm in diameter, within the surface layer. These are presumably the Pb-metal droplets which form during the hydrogen reduction of  $\text{PbO}$ .

The ISS spectra in figs. 1(a) and 1(b) show the effects of the hydrogen reduction upon the surface composition of the two glasses; the effect of acid

etching the surface before the hydrogen reduction is also shown. It can be seen that the primary effect is depletion of Pb in the surface. The sensitivity of ISS to Pb is very good – probably of the order  $10^{-3}$  to  $10^{-4}$  of a monolayer. Thus, it can be concluded that after acid etching and hydrogen reduction the Pb concentration in the surface monolayer is less than 0.01–0.1%. It is interesting that the surface depletion of lead is accomplished during the hydrogen reduction in the Cs-glass, whereas the acid-etch is required before a depletion of lead occurs in the K-glass. It has already been reported that Cs facilitates the reduction process in lead silicate glass because it creates larger holes in the glass network for the diffusion of  $\text{H}_2$ ,  $\text{H}_2\text{O}$  and Pb [31]. These data further support an effect of Cs on the transport and/or evaporation of Pb. It should be noted, finally, that there is an overlap between the Ba and Rb ISS peaks, but the complementary SIMS analyses of these specimens verify the depletion of Ba and presence of Rb in these surfaces.

The SIMS depth profiles in figs. 2(a) and 2(b) further characterize the surface layers on the two glasses after acid etching and hydrogen reduction. The most important feature is the hydrogen profile. It is not observed in the untreated fracture surface, and so there is no question that it is due to the hydrogen reduction. Initially, it was believed to correspond to the *black* surface layer, but it has been found that the ion beam crater produced during the depth profile is still *black* to a depth of  $\sim 5 \text{ }\mu\text{m}$ . On the other hand, the measured hydrogen profiles are typically 0.2–0.5  $\mu\text{m}$  in thickness. This result was surprising and was the primary motivation in attempting to use cross-sectional microscopy to measure directly the *black* layer thickness. In fact, visual observation of the ion beam crater – during sputter profiling – has provided the best estimate of *black* layer thickness; i.e.  $\sim 5 \text{ }\mu\text{m}$  for these heat treatment conditions.

The quantitative analysis of hydrogen concentration in the hydrogenated layer of the  $\text{Cs}_2\text{O}$  lead silicate glass yielded an average value of  $1.5 \times 10^{21} \text{ atom}/\text{cm}^3$ . The atomic density of this glass is  $\sim 5.3 \times 10^{22} \text{ atom}/\text{cm}^3$ . Thus, the H concentration is about 2 at.%. This is about 15% of

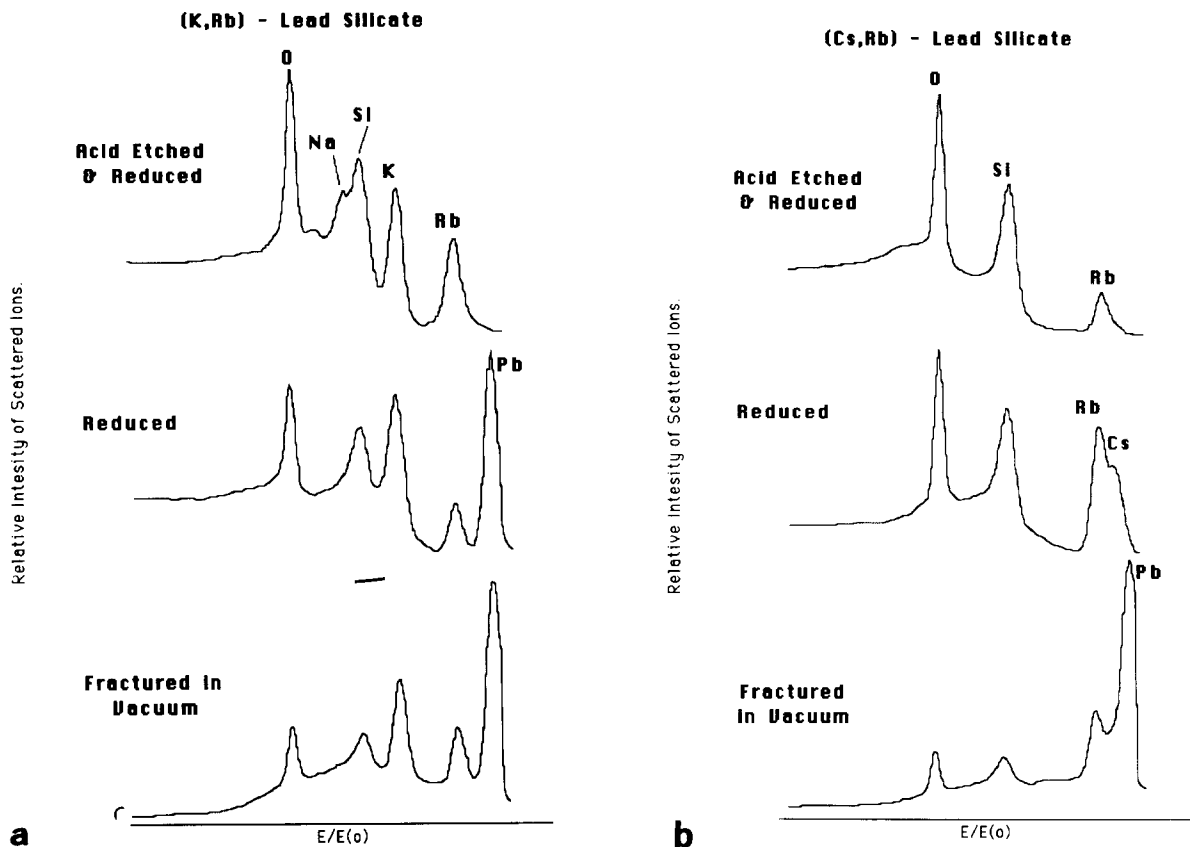


Fig. 1. (a) ISS spectra of the hydrogen heat-treated (K, Rb)-glass surfaces; the spectra of a clean fracture surface is shown for reference. (b) ISS spectra of the hydrogen heat-treated (Cs, Rb)-glass surfaces; the spectra of a clean fracture surface is shown for reference.

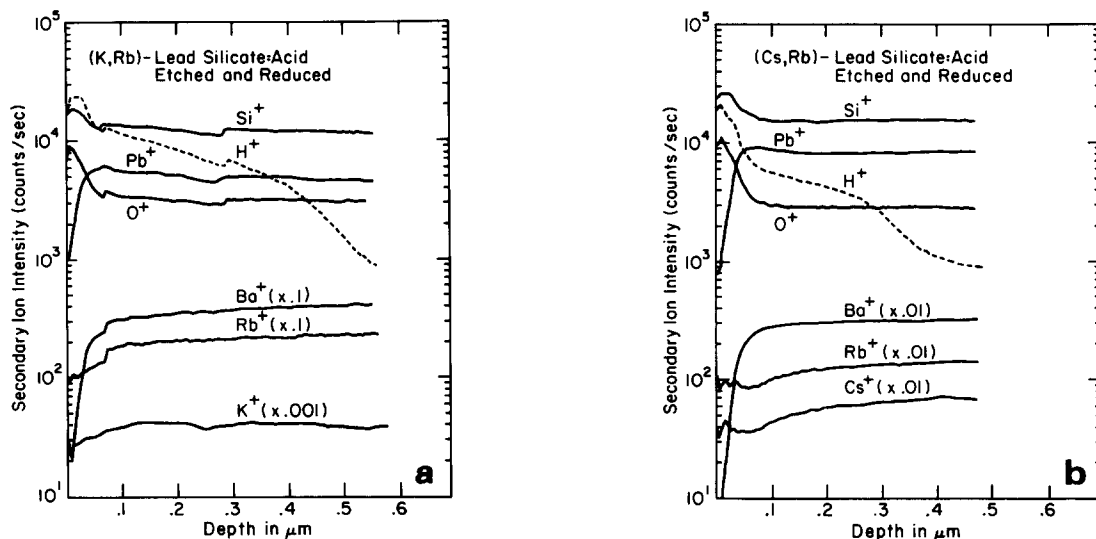


Fig. 2. (a) SIMS depth profiles of the treated (K, Rb)-glass surface. (b) SIMS depth profiles of the treated (Cs, Rb)-glass surface.

the total Pb concentration and about 3% of the O concentration. It may be significant, though, that it corresponds closely to the total Cs + Rb (~ 2.1 at.%)! Nevertheless, there is no depletion of any cationic specie, nor oxygen, over most of the range of the hydrogen profile. There is a thin zone near the surface in which Si is enriched and the Pb and Ba are depleted. In this zone, the hydrogen concentration may be considerably higher. The alkali species are also depleted over this ~ 20–50 nm thick silica-rich zone, but in contrast to the Pb and Ba these species are segregated to the outermost surface. This is consistent with the ISS spectra in fig. 1.

The XPS analyses confirmed the compositional changes observed in the ISS and SIMS analyses, but in addition, provided insight to the associated changes in the chemical structure. Figure 3 compares the high-resolution O 1s spectra for a clean surface (fractured in vacuum) with the spectra obtained after etching and hydrogen reduction. The shoulder at ~ 531.5 eV is due to the non-bridging oxygens, while the main peak at ~ 533 eV is due to the bridging oxygens. It is clear that there are no detectable non-bridging oxygens in the treated surface. The O 1s spectra of the treated surface is comparable to the spectra for  $\nu$ -SiO<sub>2</sub>, and indicates that the thermochemical depletion of Pb creates a significant structural change in the original glass network structure. The high resolution Pb 4f spectra in fig. 4 reveal only a trace of

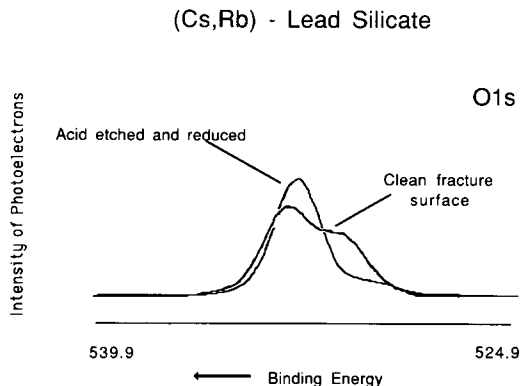


Fig. 3. High-resolution XPS spectra of the O 1s line after treatment of the (Cs, Rb)-glass; the reference spectra of a clean fracture surface shows a shoulder at lower binding energy due to non-bridging oxygen.

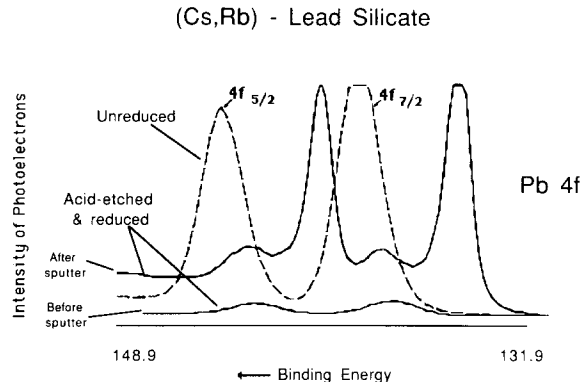


Fig. 4. High-resolution XPS spectra of the Pb 4f line after treatment of the (Cs, Rb)-glass; the spectra of a clean fracture surface is shown for reference.

Pb in the treated surface. More significant was the fact that the binding energy of this trace-level of Pb was intermediate between Pb<sup>+2</sup> and Pb<sup>0</sup>! The Pb<sup>+2</sup> line was calibrated using the clean fracture surface assuming that the Pb in the glass was PbO. Finally, the surface was subjected to a brief Ar ion bombardment to penetrate the Pb-depleted layer. Of course, one must be careful using high resolution XPS spectra after ion sputtering because of the chemical and structural damage which may occur due to the ion bombardment. However, it was nonetheless very evident that reduced lead (Pb<sup>0</sup>) was present in the subsurface. There was no observable peak due to the Pb<sup>+2</sup> in this region of the subsurface, but the Pb 4f signal due to the intermediate state of lead was greater.

Altogether, the surface analyses lead to the model which is represented schematically in fig. 5. The black surface layer is assumed to contain Pb-metal particles due to the reduction of PbO. The XPS and TEM analyses verify the presence of Pb-metal in the near surface region, but the overall thickness estimate for this layer is based solely on its *black* appearance during sputter profiling. The depth of this *black layer* extends far beyond any distinct feature in the SIMS depth profiles. A silica rich zone is observed in the outer 20–50 nm of this surface layer. Its presence is based upon the SIMS depth profiles (which show depletion of Pb, Ba, and alkali in the subsurface), and the O 1s XPS spectra (where only bridging oxygen species

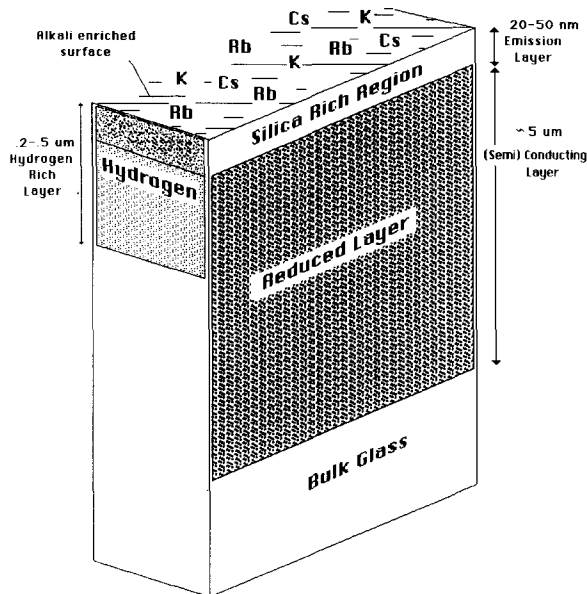


Fig. 5. Schematic representation of a typical acid-etched and reduced alkali-lead silicate glass surface; not to scale.

are detected). A thin layer of alkali species constitutes the outermost monolayer of the glass. This feature is based primarily on the ISS spectra which are most sensitive to top atomic layers of the solid, and is also consistent with the SIMS and XPS profiles. The XPS spectra do not indicate any non-bridging oxygens associated with these alkali, and so it is likely that they represent an adsorbed phase. Finally, a hydrogenated zone is observed within the surface layer. The hydrogenated zone may be duplex in nature; that is, the hydrogen concentration appears to be 2–3 times greater in the silica-rich layer. However, otherwise, the hydrogen profile does not correlate with any other elemental depth profiles, nor does it correspond to the *black layer*.

### 3.2. Electron irradiation effects

During the operation of electron multiplier and microchannel plate devices, the reduced glass surfaces are exposed to electron bombardment. This electron irradiation can modify or otherwise damage the surface through a variety of mecha-

nisms. The net effect can be one or more of the following:

- (1) changes in surface composition,
- (2) structural modification or damage,
- (3) generation/annihilation of electronic defects,
- (4) electrical charging, and
- (5) heating.

The mechanisms and effects of electron interactions with solid surfaces have been reviewed in detail elsewhere [32]. Of particular concern, here, are the possible effects of electron stimulated desorption (ESD), electron stimulated adsorption (ESA), and electromigration. These phenomena can oxidize the surface, deposit carbonaceous layers on the surface, or influence the concentration and depth distribution of alkali ions in the reduced glass surface layer. The surface composition will affect the surface work function and, thereby, is a critical factor in the secondary electron yield. Hill [7] has shown an effect of potassium upon the secondary electron yield of alkali-lead silicate glasses and, moreover, he suggested that electron-induced changes in the potassium surface concentration might be responsible for the gain instability of devices. In other studies, the external effects of  $H_2O$  [33] and hydrocarbon impurities [21] in the vacuum environment were related to changes in the gain of the device. The effects of external contamination are clearly of importance, but in the present study, the intrinsic effects on the *clean reduced glass surface* were of primary interest.

The specific objective of these experiments was to measure, in situ, any changes in the alkali surface concentration during electron irradiation. The extent of the change was measured as a function of the accumulated electron dose, the glass composition, and the surface treatment. Although many studies of electron *beam* damage in glass surfaces have been reported [32] because of their effect upon electron microprobe and Auger analyses, the exposure here used low energy electrons ( $\sim 500$  eV) at low current density ( $\sim 1-5 \times 10^{-6}$  A/cm<sup>2</sup>) to simulate the conditions in real devices. ISS was used to monitor the surface composition due to its monolayer sensitivity to alkali. It was determined in an independent set of experiments that the ion beam used to obtain the ISS

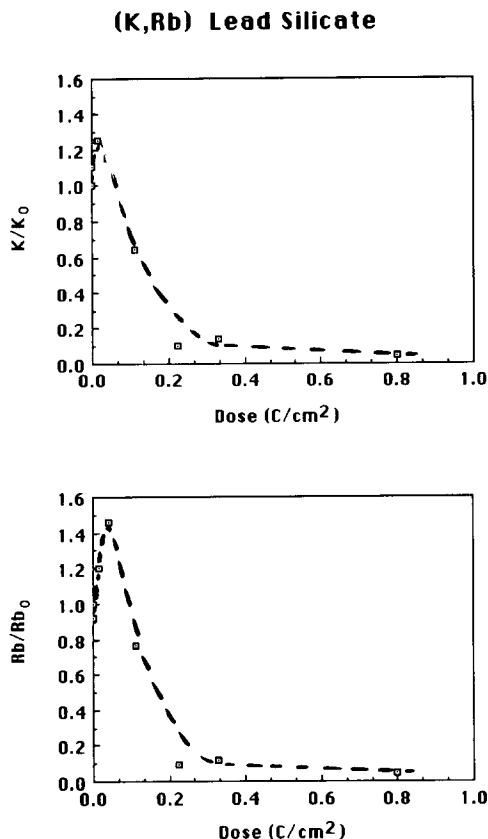


Fig. 6. (a) The measured changes in the ISS alkali signals due to electron irradiation (at 500 eV) of the acid-etched and reduced (K, Rb)-glass.

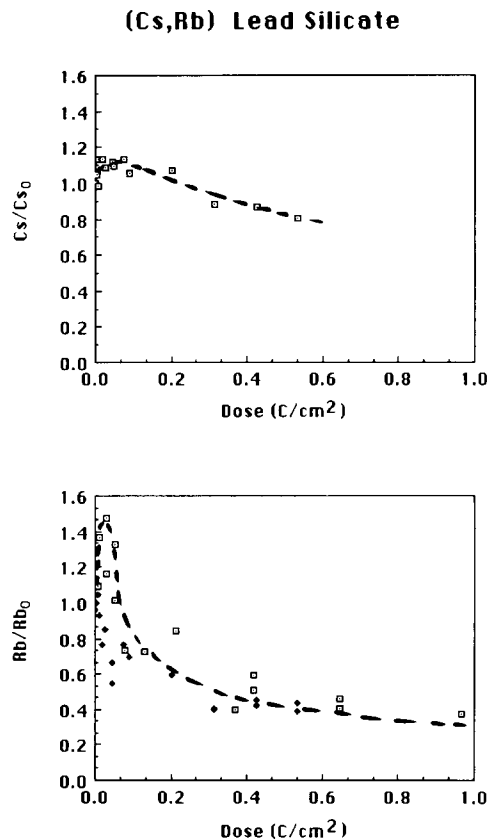


Fig. 6. (b) the measured changes in the ISS alkali signals due to electron irradiation (at 500 eV) of the acid-etched and reduced (Cs, Rb)-glass; the filled points in the lower plot are for a reduced surface w/o acid etching.

spectra does not change the surface composition over the time-scale of the analysis.

The primary effect of the electron irradiation was a decrease in the alkali and lead surface concentration. The time-dependent change was considerably more rapid for the alkali than for the lead. In the case of *unreduced* fracture surfaces (created in vacuum), the effect was not very large – even though the initial concentrations of alkali and lead are high. In the reduced surfaces, however, the alkali (and lead, in the case of the K,Rb-glass) concentrations were reduced by 50% to 100% after a dose of the order 1  $C/cm^2$ . Figures 6(a) and 6(b) compare these changes in alkali for the (K, Rb)- and (Cs,Rb)-glasses, respectively. Clearly, the (K,Rb)-glass is more susceptible to the beam-induced reduction in alkali surface concentration

than the (Cs,Rb)-glass. In both glasses, though, there is an increase of alkali signal during the initial stages of electron irradiation which may be due to desorption of water or hydrocarbon impurities.

#### 4. Discussion

The data in fig. 6 were fit to established models for electron-stimulated effects at surfaces; i.e., the first-order relation:

$$C(t) = C(0) \exp - [DQ/e],$$

where  $C(0)$  is the initial surface concentration of alkali species,  $C(t)$  is the alkali concentration at time =  $t$ ,  $D$  is the electron dose,  $e$  is the electron

Table 1  
Excitation cross-sections ( $Q$ ) and critical doses ( $D_c$ ) for electron-stimulated changes in surface composition

	$Q$ (cm <sup>2</sup> )	$D_c$ (C/cm <sup>2</sup> )
Potassium-lead silicate glass (at 500 eV)		
– clean surface	$8.7 \times 10^{-20}$	0.20
– acid etched/reduced surface	$1.2 \times 10^{-18}$	0.01
Cesium-lead silicate glass (at 500 eV)		
– clean surface	$5.6 \times 10^{-20}$	0.31
– acid etched/reduced surface	$2.2 \times 10^{-19}$	0.08
Silicon dioxide (at 2000 eV)	$2.9 \times 10^{-20}$	0.60
Potassium chloride (at 1500 eV)	$5.9 \times 10^{-19}$	0.03
Benzene-on-Ru (at 1500 eV)	$8 \times 10^{-17}$	0.0002
CO-on-Pt (at 1500 eV)	$5 \times 10^{-18}$	0.003
O <sub>2</sub> -on-Ti (at 300 eV)	$5 \times 10^{-19}$	0.03

charge ( $1.6 \times 10^{-19}$  C), and  $Q$  is the effective cross-section for the electron stimulated change in surface composition,  $\Delta C$ . The model implicitly assumes that the change in alkali surface concentration is due to their electronic excitation by the incident electrons. The electron dose,  $D$  (in C/cm<sup>2</sup>), is simply a product of the current density of incident electrons  $J$  (in A/cm<sup>2</sup>) and the total time of irradiation  $t$ . Thus, the cross-sections for the excitation process can be determined using the data in fig. 6. These cross-sections are presented in table 1, along with data reported in the literature [32] for other materials. The fact that the data in fig. 6 fit the relation, and yield cross-sections of the order  $10^{-17}$  to  $10^{-19}$  cm<sup>2</sup>, is consistent with the phenomena of electron stimulated desorption (ESD). Table 1 also presents a parameter termed the critical dose,  $D_c$ . This corresponds to the cumulative electron dose that is required to change the alkali surface concentration – in the surface monolayer – by 10%. The critical doses for composition changes in other materials are shown for comparison.

It can be seen in table 1 that the critical doses for alkali desorption in the *reduced* glasses are much less than in the *unreduced* glasses. It is also apparent that the critical doses for the *reduced glasses* are in the range of adsorbates on solid surfaces. The comparison indicates that the alkali on the *reduced* surfaces may be adsorbed, whereas

the alkalis in the *unreduced* fracture surfaces are integral to the glass network structure. It is also evident that the susceptibility to the effect is  $\sim 10 \times$  greater for the K-glass. This compositional effect is not easy to rationalize on the basis of ESD. Nevertheless, the direct analysis of the desorption flux during electron irradiation of these glasses verifies the ejection of alkali species. A determination of the relative rates of Cs, K, and Rb desorption in the two glasses is currently underway.

One can further interpret the observed decrease in alkali surface concentration on the basis of electromigration. There are many examples of alkali diffusion in or out of the surface of glass due to the electric fields created by the electron irradiation. A transport phenomenon would be consistent with the higher rate of change in the K versus the Cs. In fact, the combined effects of electromigration and ESD could explain the initial increase in the alkali concentration: i.e. a diffusion limited electromigration of alkali to the surface monolayer where it is subject to ESD. There are models which quantitatively describe a combined ESD/electromigration mechanism during electron beam irradiation of glasses [32] and these also yield an effective cross-section of the order  $10^{-18}$  cm<sup>2</sup>. Moreover, the SIMS in-depth profiles of the alkali and hydrogen were found to be influenced by the electron bombardment. But clearly, more work will be necessary to determine the relative magnitudes of the electron-stimulated desorption and electromigration.

## 5. Summary

The effects of hydrogen reduction, acid etching and electron irradiation upon the surface composition of (K,Rb)-lead silicate and (Cs,Rb)-lead silicate glasses have been investigated. The reduction of Pb may occur over depths of the order 5  $\mu$ m, and it is probably this layer that is responsible for the conductivity. However, the secondary electron emission arises in, at most, the outermost 1.0–10.0 nm of the surface. Within this zone, the primary effect of the hydrogen reduction is the depletion of the alkali and lead, and the conse-

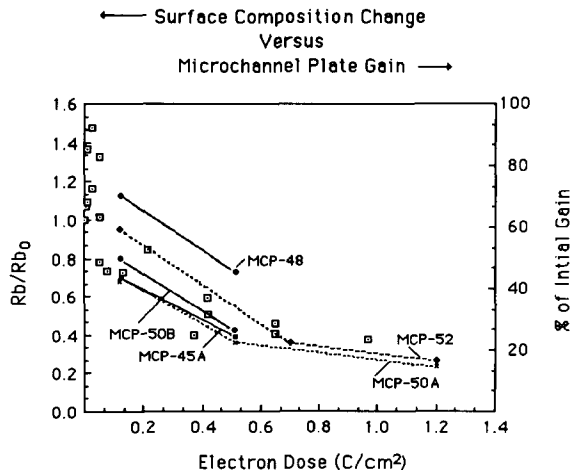


Fig. 7. The dose-dependent changes in the gain of various MCP devices (solid connected points), and the Rb surface concentration on acid-etched and reduced fracture surfaces (open points); the MCPs and the fracture surfaces are (Cs, Rb)-lead silicate.

quent creation of a silica-rich region. The surface monolayer of this silica-rich region is enriched in alkali – presumably adsorbed alkali species – although the *bulk* of the silica-rich region also contains a small concentration of alkali. The hydrogen profile does not correlate directly with any compositional feature of the surface. There is no question that it arises due to the hydrogen reduction, but its role in the emission and/or emission stability has not yet been established.

Not surprisingly, the primary effect of electron irradiation was found to be a change in the alkali surface concentration. The significance of these in situ electron irradiation experiments is revealed in fig. 7. Here, the electron dose-dependent changes in the gain of some real microchannel plate devices are plotted together with the alkali surface composition changes measured in this study. It seems clear that the ranges of electron dose over which the gain of the devices decreases correspond closely to those which cause changes in alkali surface concentration. These doses exceed those which are responsible for the initial ‘clean-up’ of adsorbed water, hydrocarbon and hydrogen (usually 0.01–0.1 C/cm<sup>2</sup>). It implies that the long-term gain of the devices relates more directly to a *steady-state surface concentration of alkali*, the

magnitude of which depends upon the relative rates of desorption, electromigration, and out-diffusion through the silica-rich zone. This steady state concentration would be determined by the thickness of the silica-rich region, the type(s) of alkali (that is, their diffusivity and solubility in the silica-rich zone), the bulk concentration of alkali, and, of course, the flux and energy of incident electrons. It is implicit that these latter factors are critical not only to the long-term gain and stability of the device, but also to the useful life of the device. Altogether, these studies point to the need for further verification of the ESD/electromigration model and, correspondingly, the dependence of the rate constants upon the glass composition. In this way, predictions of the long-term stability and life of the devices could be established.

The authors gratefully acknowledge the financial support, and supply of materials, provided by Galileo Electro-Optics Corporation.

## References

- [1] R.L. Green and K. Blodgett, *J. Am. Ceram. Soc.* 31 (1948) 89.
- [2] K.B. Blodgett, *J. Am. Ceram. Soc.* 34 (1951) 14.
- [3] E.A. Fainberg, *Izv. Akad. Nauk SSSR, Neorg. Mater.* 2 (1966) 1154.
- [4] J.J. Genco and B.C. Almaula, *Ceram. Bull.* 48 (1969) 846.
- [5] E.A. Fainberg, *Zh. Prikl. Khim.* 38 (1965) 2192.
- [6] C.W. Bates Jr., J. Helmer and N. Wiechert, *Solid State Commun.* 10 (1972) 847.
- [7] G.E. Hill, *Adv. Elect. Elect. Phys.* 40A (1976) 153.
- [8] A. Authinarayanan and R.W. Dudding, *Adv. Elect. Elect. Phys.* 40A (1976) 167.
- [9] R.L. Verma, *J. Phys. D* 10 (1977) 1735.
- [10] S.H. Siddiqui, *J. Appl. Phys.* 48 (1977) 3053.
- [11] D.K. Sattarov, Z.I. Kanchiev, G.Ya. Konaeva and K.P. Pecherskaya, *Zh. Prikl. Khim.* 51 (1978) 933.
- [12] A.M. Tyutikov, N.V. Lobanova, M.N. Toiseva, V.N. Polukhin, N.V. Korolev and V.E. Yakovlev, *Fiz. Khim. Stekla* 5 (1979) 628.
- [13] A.M. Tyutikov, N.V. Korolev, M.N. Toiseva, L.V. Petukhova and A.S. Kharin, *Opt. Mekh. Promst.* 47 (1980) 11.
- [14] G.T. Petrovskii, D.K. Sattarov and Z.I. Kanchiev, *Fiz. Khim. Stekla* 7 (1981) 457.
- [15] O.M. Artamonov, D.K. Sattarov, O.M. Smirnov, A.N. Terekhov, V.A. Kar'yuzov and G.A. Cheban, *Fiz. Khim. Stekla* 7 (1981) 470.

- [16] A.M. Tyutikov, M.N. Toiseva, V.N. Polukhin, N.V. Lobanova and V.E. Yakovlev, *Fiz. Khim. Stekla* 7 (1981) 705.
- [17] Ju.M. Simeonova, J.S. Kourtev and Y.B. Dimitriev, *J. Non-Cryst. Solids* 57 (1983) 177.
- [18] L.A. Gravel', N.B. Leonov, Yu.B. Novikov, M.N. Toiseva and A.M. Tyutikov, *Fiz. Khim. Stekla* 10 (1984) 75.
- [19] L.N. Kapitonova, V.A. Khar'yuzov, V.A. Nikitin and B.M. Zolotarev, *Fiz. Khim. Stekla* 11 (1985) 193.
- [20] O.M. Artamonov, Yu.P. Kostikov, V.A. Novolodskii, I.V. Redina, D.K. Sattarov, O.M. Smirnov, A.N. Terekhov and V.A. Khar'yuzov, *Fiz. Khim. Stekla* 11 (1985) 326.
- [21] S.A. Eliseev, V.A. Novolodskii, O.M. Smirnov, A.N. Terekhov and V.A. Khar'yuzov, *Fiz. Khim. Stekla* 12 (1986) 461.
- [22] H.J.L. Trap, *Acta Electronica* 14 (1971) 41.
- [23] J.N. Sandoe, P. Blood and D.H. Nicholls, *Appl. Phys. Lett.* 37 (1980) 334.
- [24] O. Gzowski, L. Murawski and K. Trzebiatowski, *J. Non-Cryst. Solids* 41 (1980) 267.
- [25] O. Gzowski, L. Murawski and K. Trzebiatowski, *J. Phys. D* 15 (1982) 1097.
- [26] Yu.M. Simeonova, E. Gattef, Y.B. Dimitriev and J.S. Kourtev, *Int. J. Electron.* 58 (1985) 351.
- [27] J.L. Wiza, *Nucl. Instr. and Meth.* 162 (1979) 587.
- [28] D.K. Sattarov, Z.I. Kanchiev, G.Ya. Konaeva and L.S. Trofimova, *Zh. Prikl. Khim.* 52 (1979) 1981.
- [29] A.M. Tyutikov, *Sov. J. Opt. Technol.* 41 (1974) 413.
- [30] N.R. Rajopadhye, S.V. Bhoraskar and D. Chakravorty, *J. Non-Cryst. Solids* 105 (1988) 179.
- [31] I.I. Kitaigorodskii, D.I. Mendeleev, E.A. Fainberg and L.A. Grechanik, *Steldo Keram.* 19 (1962) 8.
- [32] C.G. Pantano and A.M. Then, to appear in *Methods and Phenomena* (Elsevier, Netherlands, 1989).
- [33] M. Lichtensteiger and C. Webb, *J. Vac. Sci. Technol. A2* (1984) 1513.